NACA

RESEARCH MEMORANDUM

INVESTIGATION OF A 10-STAGE SUBSONIC AXIAL-FLOW

RESEARCH COMPRESSOR

III - INVESTIGATION OF ROTATING STALL, BLADE VIBRATION
AND SURGE AT LOW AND INTERMEDIATE COMPRESSOR

SPEEDS

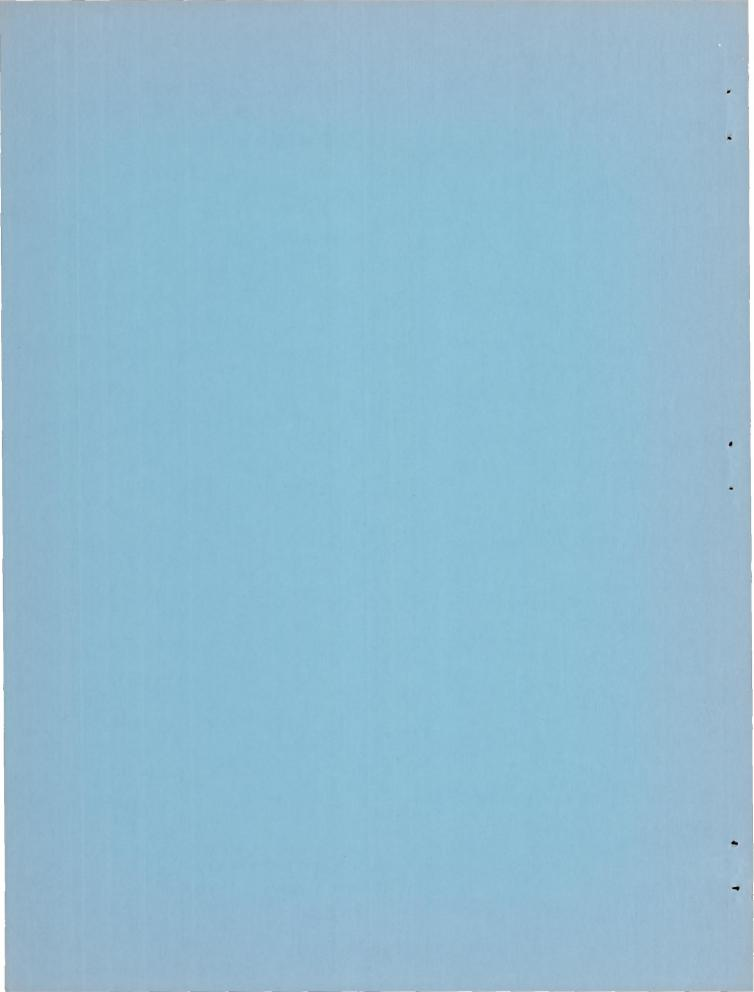
By Merle C. Huppert, Eleanor L. Costilow, and Ray E. Budinger

Lewis Flight Propulsion Laboratory Cleveland, Ohio

NATIONAL ADVISORY COMMITTEE FOR AERONAUTICS

WASHINGTON

May 18, 1953 Declassified June 24, 1958



NATIONAL ADVISORY COMMITTEE FOR AERONAUTICS

RESEARCH MEMORANDUM

INVESTIGATION OF A 10-STAGE SUBSONIC AXIAL-FLOW RESEARCH COMPRESSOR

III - INVESTIGATION OF ROTATING STALL, BLADE VIBRATION, AND SURGE

AT LOW AND INTERMEDIATE COMPRESSOR SPEEDS

By Merle C. Huppert, Eleanor L. Costilow, and Ray E. Budinger

SUMMARY

An investigation of rotating stall and surge at low and intermediate speeds was conducted on a 10-stage subsonic axial-flow research compressor. The fluctuations of rotating stall and surge were detected by hot-wire anemometers and pressure transducers.

At 50 percent of design speed the flow fluctuations accompanying rotating stall were found at all weight flows. The number of stall regions in the stall pattern varied from three at the highest weight flow investigated to seven near the surge point. At 60 percent of design speed only the stall patterns with three and four stall regions were obtained, and at 70 percent of design speed only the stall pattern with three stall regions was found. For all stall patterns obtained, the stall regions revolved about the compressor axis in the direction of compressor rotation at about 57 percent of compressor speed.

The amplitude of the flow fluctuations of stall was greatest in the first four stages and diminished somewhat in the latter stages. In the first four stages the amplitude of the fluctuations was greatest at the tip section and somewhat less at the hub section.

An analysis of the possibility of compressor blade vibration indicated that only the inlet guide vanes and first stator were in danger of fatigue failure from resonant vibrations excited by rotating stall. The inlet guide vanes were the only blades to exhibit fatigue cracks during the course of the investigation of this compressor.

The hot-wire anemometer and pressure transducer data obtained during surge at 50 percent of design speed indicate that the surge pulse was initiated by a general breakdown of flow in the compressor which results in a rotating stall pattern with a single-stall region extending from the compressor inlet to the compressor exit. At the minimum flow rate during a surge pulse the stall region spread circumferentially to cover the complete annulus of the compressor. The flow rate then

increased to a value greater than that at which stall occurred and the compressor was momentarily relieved of stall, at which time the flow rate first increased considerably and then gradually decreased to the value for stall and the cycle was repeated. The compressor discharge pressure drop during a surge pulse was 75 percent of the pressure rise prior to surge.

INTRODUCTION

Operation of multistage axial-flow compressors at low and intermediate speeds generally results in stall of the inlet stages. Reference l presents a discussion of the variation of inlet stage flow coefficient with compressor rotational speed and weight flow and shows that stall in the inlet stages may exist over a large part of the compressor operating range at low compressor speeds.

Stall of any stage of a compressor may produce large spacial periodic flow fluctuations within the compressor. References 2 to 4 establish the cause of these flow fluctuations to be the low flow regions within the compressor that rotate about the compressor axis, generally in the direction of rotor rotation. The single-stage data presented in references 4 and 5 indicate that the rotational speed of the stall regions is proportional to the compressor rotational speed and that the ratio of the rotative speed of the stall regions to the rotor speed depends on the number of equally spaced stall regions in the stall pattern.

Rotating stall is of importance in several present-day compressor problems. Stall of one stage in a multistage compressor may deteriorate the performance of several adjacent stages, as discussed in references 6 and 7. Unfavorably shaped surge lines and poor efficiency at low and intermediate speeds are evidently influenced by the magnitude and type of rotating stall and attendant stage interaction effects. Reference 5 has established that resonant vibration of compressor blading can be excited by rotating stall. The investigation (ref. 5) was conducted on a single-stage compressor so that the complete significance of rotating stall in vibration problems with multistage compressors has not been established.

The purpose of the investigation made at the NACA Lewis laboratory and reported herein was to study rotating stall in a 10-stage axial-flow compressor and to investigate the connection between stall and surge. Conditions at which resonant blade vibrations excited by rotating stall were likely were also determined.

Hot-wire anemometer measurements of the flow fluctuations of rotating stall were made at the tip, mean, and hub radii in the first, second,

third, fourth, fifth, seventh, and tenth stages at 50, 60, and 70 percent of design speed. The flow fluctuations of surge were measured at 50 percent of design speed with pressure transducers and hot-wire anemometers.

SYMBOLS

The following symbols are used in this report:

A, C, E	refer to radial stations (see table I)
fb	natural bending frequency of compressor blade
$(f_b)_n$	natural bending frequency at any rotor speed
(f _b) _{st}	natural bending frequency at stationary conditions
f _S	frequency with which stall regions pass anemometer probe
h	rotational speed of stall regions, rps
N	compressor rotational speed, rps
P	stagnation pressure, lb/sq in.
r	ratio of local radius to tip radius
V	velocity, ft/sec
w	weight flow, lb/sec
X	time increment on oscillogram between appearance of stall at one anemometer station and appearance of stall on other anemometer
Y	f _S X
z	axial distance, in.
α	angle between two anemometer probes
δ	ratio of stagnation pressure at compressor inlet P _O to standard pressure of 14.7 lb/sq in.
ΔP_{c}	compressor pressure rise at surge point

change in stagnation pressure during surge

 ΔP_{S}

$\frac{\triangle \nabla \Lambda}{\Delta \Delta}$	average peak to peak variation in weight flow rate divided by weight flow rate based on time average current through anemometer probe
ε	angle of spiral of stall region (see fig. 16)
0	ratio of stagnation temperature at compressor inlet $\rm T_{0}$ to standard temperature, 518.6 $^{\rm o}$ R
λ	number of stall regions in stall pattern
υ	angle between stall regions
ρ	density, lb/cu ft
ρV	weight flow rate, lb/(sq ft)(sec)
$\overline{\rho V}$	weight flow rate based on time average current through anemometer probe
Subscripts:	
0,2,3,	refer to axial station in compressor (see fig. 1)
Superscripts:	
1	relative to rotor blading
11	value based on signals from anemometer probes at different axial stations

APPARATUS, INSTRUMENTATION, AND PROCEDURE

Apparatus. - The compressor used for this investigation was a 20-inch tip diameter, 10-stage subsonic axial-flow research compressor designed for a pressure ratio of 6.45 and an equivalent weight flow of 57.5 pounds per second. The compressor was designed for symmetrical velocity diagrams and approximately constant stagnation enthalpy increase at all radii. A detailed study of the aerodynamic design is presented in reference 8 and a preliminary analysis of the over-all performance and a description of the test facility and instrumentation used for obtaining over-all performance is given in reference 9.

Instrumentation. - The flow fluctuations of rotating stall were detected and measured by constant-temperature hot-wire anemometers. The anemometer system used is described in reference 10. The anemometer

probes used were wired with 0.0002-inch-diameter tungsten wire with an unplated length (effective length) of 0.08 inch. The wire element of the probes used was mounted perpendicular to the probe axis.

Anemometer probes were installed in radial survey devices at eight axial stations between 2 through 22 as shown in figure 1 (station numbering system is the same as that used in ref. 9). The wire element was oriented normal to the flow direction determined by an angle measuring device. Two or more probes were installed at stations 2, 3, and 10, with one probe in a circumferential survey device at each of these stations in order to facilitate the determination of the number of stall regions in the annulus at each operating condition (see ref. 4). The number of stall regions was determined at three axial stations in order to determine whether the number of stall regions was the same at all axial stations. The radial surveys were made to determine the radial variation in amplitude of the flow fluctuations of rotating stall. The radial positions at each axial station where data were taken are given in table I.

The anemometer signals were viewed or photographed two at a time on a dual-beam oscilloscope. The frequency with which stall regions passed an anemometer station was determined by forming Lissajous figures with the aid of an audio-frequency oscillator (see ref. 11).

Strain-gage-type pressure transducers were installed at axial stations 0, 23, and 24 of figure 1 to measure the static- and stagnation-pressure fluctuations during surge. Casing static and stagnation pressure fluctuations at midpassage were measured at station 0. At the compressor discharge, outer wall static-pressure fluctuations during surge were measured at station 23 and midpassage stagnation pressure fluctuations were measured at station 24. The pressure transducer signals obtained during surge were recorded along with an anemometer signal on a recording oscillograph.

Procedure. - At 50, 60, and 70 percent of design speed the weight flow rate through the compressor was varied from that value at which the compressor discharge static pressure was approximately equal to the compressor inlet stagnation pressure to the value at which surge occurred. Radial and circumferential surveys were taken at the highest weight flow rate at which any given stall pattern could be obtained. The number of stall regions in each stall pattern and the amplitude of the flow fluctuation were determined by the methods outlined in reference 4. Inasmuch as the stall regions may extend some distance axially through a compressor, it is of interest to know the extent of the spiraling motion of a stall region as it passes through a compressor. The method used to determine the angle of spiral is given in appendix A.

RESULTS AND DISCUSSION

Over-All Performance and Rotating Stall

Following the investigation reported in reference 9, inspection of the compressor revealed cracks in the inlet guide vanes which necessitated their replacement. The over-all characteristics of the compressor with the new set of inlet guide vanes are shown in figure 2. The performance was substantially the same as with the original set of guide vanes (ref. 9). Additional surge point data obtained in the speed range between 70 and 80 percent of design speed revealed a slight knee in the surge line in this speed range.

Stall patterns. - The radial and circumferential survey with hotwire anemometers at compressor speeds of 50, 60, and 70 percent of design speed indicated the presence of rotating stall in the compressor. The weight flow and speed range for each stall pattern obtained and the number of stall regions in each stall pattern are shown in figure 3. Although the point of transition from one stall pattern to another was determined several times for each stall pattern and at each speed, some small variations in the data were evident. The contours on figure 3 indicate the highest weight flow at which each stall pattern was observed. Inasmuch as the contours separating the operating regions for each number of stall regions are based on only one point or, at the most, two points, they must be considered approximate. At 50 percent of design speed, three stall regions were found at the highest weight flow investigated. As the weight flow was reduced the number of stall regions increased from three to four, from four to five, and so on up to seven stall regions near the surge point as indicated. At 60 percent of design speed there were no fluctuations of rotating stall at the highest weight flow investigated. As the weight flow was reduced, rotating stall with three stall regions in the stall pattern was obtained, as shown in figure 3. As the weight flow was further reduced the number of stalls changed from three to four. The pattern with four stalls remained up to the surge point.

At 70 percent of design speed only the stall pattern with three stalls was found. At the weight flow where this stall pattern was first obtained the fluctuations were intermittent, that is, they appeared and disappeared on the oscilloscope screen, possibly because of a mild inaudible instability surge, but became quite regular as the flow was further reduced to the value indicated in figure 3. From the contours of constant λ and the surge line in figure 3, it is apparent that rotating stall would not be obtained in the surge-free operating range above about 75 percent of design speed. The following table summarizes the data obtained with regard to the frequency with which a stall region passed an anemometer probe fg, the number of stalls in each stall pattern λ , the rotational speed of the stall regions h, and the ratio of stall speed to compressor speed $h/N/\sqrt{\theta}$:

7

Design speed, percent	compressor	Frequency with which stall region passed anemometer probe (all axial stations), f _S , cps	Number of stall regions in stall pattern (determined at axial stations 2, 3, and 10),	Rotation speed of stall regions, $h = \frac{f_S}{\lambda},$ rps	Stall speed to rotor speed ratio, $\frac{h}{N/\sqrt{\theta}}$
50	82.9	142 190 240 290 340	3 4 5 6 7	47.3 47.5 48.0 48.3 48.6	0.571 .573 .579 .583 .586
60	99.6	168 228	3 4	56.0 57.0	0.562
70	116.6	198	3	66.0	0.566

As shown in the table the rotational speed of the stall regions was approximately 0.57 of the compressor rotational speed for all the data obtained. The single-stage compressor data presented in reference 6 indicated an increase in rotative speed of the stall regions with the number of stall regions formed.

The number of stall regions λ in each stall pattern was the same at axial stations 2, 3, and 10, and the frequency f_S with which a stall region passed an anemometer station for any given stall pattern was the same at all axial stations at which data were obtained.

The extent to which the stall regions spiraled as they passed through the compressor was determined from the oscillograms of the anemometer signals by the method outlined in appendix A. The accuracy of interpreting the oscillograms to determine the angle ϵ (see appendix A) was probably $\pm 15^{\circ}$, and the angle ϵ computed from the oscillograms did not exceed $\pm 15^{\circ}$ in any case, indicating little or no spiraling of the stall regions.

These data indicate that the stall regions were equally spaced and extended completely through the compressor and that the stall patterns were rotating about the axis of the compressor as a solid body with little, if any, spiraling motion.

Variation of wave form and amplitude of stall fluctuations with axial and radial position. - A typical set of oscillograms obtained at 60 percent of design speed with four stall regions in the stall pattern (compressor operation points F and G, fig. 3) is shown in figure 4. In each oscillogram the top trace is from an anemometer probe at axial

8

station 2 (behind first rotor). The figure shows a comparison for three radial positions (tip, mean, and hub positions) of the amplitude and wave form of the flow fluctuations at axial stations 7 (after third stator), 10 (after fifth rotor), 15 (after seventh stator), and 22 (after tenth stator) with those at axial station 2 (after first rotor). The amplitude of the fluctuations varies considerably from the tip (radial station A) to the hub (radial station E) at axial stations 2 and 7 and is nearly the same at the tip (radial station A) and hub (radial station E) at axial stations 10, 15, and 22.

The variation in wave form and amplitude of the fluctuation among the top traces (all obtained at axial station 2) indicates the unsteady nature of stall regions with regard to wave form and amplitude of the fluctuations. The harmonics of the fundamental of the stall frequency f_S were attenuated more than the fundamental as the stall region passed beyond axial station 10, and the fluctuations are nearly sinusoidal in wave form at axial stations 12 and 22 (see figs. 4(h) to 4(1)), indicating a mixing and spreading of the air originally involved in stall.

The variation of the amplitude of the fluctuations of stall with axial and radial position for each stall pattern observed at the speeds investigated is given in figures 5, 6, and 7 (50, 60, and 70 percent of design speed, respectively). In some cases the lines joining the data points are dashed, indicating lack of data in these regions. The amplitude of the flow fluctuation $\Delta \rho V/\rho V$ at each axial station investigated divided by $(\Delta \rho V/\rho \overline{V})_{2A}$ (radial station A at axial station 2) is plotted against axial distance measured from a station 1 inch upstream of the inlet guide vanes. Each data point is the average of several oscillograms, and consequently the figures represent the average axial variation in amplitude of the stall region for each stall pattern obtained. The largest fluctuations occurred in the second, third, and fourth stages (axial measuring stations 5, 7, and 9) and the amplitude was considerably reduced in the exit stages. The fluctuations behind the first rotor (axial station 2) were not so large as those in the second, third, and fourth stages; and a rather sharp reduction in amplitude occurred across the fifth rotor (axial station 10).

A comparison of figures 5, 6, and 7 indicates that the amplitude of the fluctuations in the last stage are larger with respect to the inlet stage at 70 percent of design speed than at 50 percent of design speed.

In general, it was not possible to determine which stage initiated the rotating stall pattern. In most cases, if the fluctuations of rotating stall could be detected in one stage of the compressor they could also be detected in any other stage at the same frequency fg. However, at 40 percent of design speed at a high weight flow, rotating stall was clearly indicated behind the second stator (axial station 5) but not detectable at all behind the first rotor (axial station 2) or at any

other axial station at which probes were located. The higher amplitudes in the first four stages indicate that the rotating stall originated in these stages as would be expected from stage matching considerations (see refs. 1 and 7). Inasmuch as the fluctuations behind the first rotor (axial station 2) were smaller in amplitude than at axial stations 5 and 7, it may be concluded that either the stall did not originate in the first stage or if it did the fluctuations were amplified in the second and third stages.

The rotating stall patterns obtained were of the type caused by a gradual stall along the blade span initiated by a rotor tip stall of one of the first three or four stages. This type of stall is referred to as progressive stall in reference 7 and results in a gradual decrease in stage pressure coefficient with reduction in flow coefficient as contrasted with the discontinuous drop in pressure coefficient obtained with simultaneous stall at all radii (see refs. 4 and 7).

Effect of stator wake on anemometer signal. - The wave form of a stall region as indicated by an oscillogram was quite independent of circumferential position at stations 2 and 10, which were behind rotors. Behind the first stator (axial station 3), however, the wave form was affected considerably by the position of the anemometer probe with respect to a stator blade wake. This effect is shown in figure 8. The top trace in each oscillogram is from a probe located midway between stator blades. In figure 8(a), the angular spacing of wires α was 86° and, because there were four stall regions in the stall pattern $(\lambda = 4)$, the fluctuations should appear nearly in phase, as shown. As the probe producing the lower trace was moved angularly to increase a toward 90° so that the fluctuations would appear in phase on the oscilloscope, the wave form changed considerably, as shown in figure 8(b) where $\alpha = 88^{\circ}$. At this value of angular spacing the stall regions appear to be a region of increase of weight flow rate rather than a decrease. In figure 8(c) where α is 92°, the indication of rotating stall on the lower trace is rather indefinite. Because of this effect the circumferential survey data obtained behind the second stator (axial station 3) were not used in the determination of the number of stalls unless the angular spacing of the probes was such that both probes were approximately midway between blades. Evidently the flow pattern within a stall region has a pronounced effect on the blade wakes contained within the stall region.

Rotating Stall and Blade Vibration

The data of reference 5 show that rotating stall can excite compressor blading to resonant vibration which may result in blade failure. Consequently, a study was made to determine at which compressor speeds and weight flows resonant vibration of blades excited by rotating stall was likely to occur.

As discussed earlier in the report the stall frequency fs increased practically linearly with speed for any particular stall pattern and, in fact, the rotational speed of the stall regions was nearly independent of the number of stall regions in the stall pattern. The average fundamental bending frequencies of several of the blades in each blade row were determined experimentally and the values are given in table II.

The fundamental bending frequency of rotor blades increases with rotational speed because of the stiffening effect of centrifugal force. The method used for approximating the effect of centrifugal force on bending frequency is given in appendix B.

The ratio of the stall frequency to the blade fundamental frequency for the inlet guide vanes, the first stator, and the first rotor plotted against rotor speed in percent of design speed is presented in figure 9 for each stall pattern obtained. For the stator blades this ratio is f_S/f_b and for the rotor blade, $f_S'/(f_b)_n$ where $f_S' = (N-h)\lambda = \lambda N - f_S$. In the case of the stator blades the contours for various values of λ are straight lines passing through the origin and in the case of the rotor blades they are curved lines because of the increase of (fb)n with compressor speed. Horizontal lines indicating the ratio at which resonance may occur with the fundamental stall frequency or its first two harmonics are included. The compressor speeds at which resonance may occur are indicated by the intersection of the horizontal lines and the stall frequency lines. The surge limiting line included indicates the compressor speeds at which lines separating the various stall patterns intersect the surge line in figure 3. A similar analysis was made of the stator and rotor blades through the fifth stage. The following table summarizes the resonant vibration conditions determined. It is shown that the inlet guide vanes and first stator blades are the only blade rows that could be excited to resonance by the fundamental of the stall frequency fs or fs'. Resonance with the fundamental would occur at 44 and 59 percent of design speed in the inlet guide vanes and at 41.5 and 49 percent of design speed in the first stator blades.

Blade row	Number of stall regions in stall pattern,	Speed at which resonance is indicated in percent design speed		
even securities even securities tos sufficient to	A Tree A A Loring to the last of the last	Fundamental	First harmonic	Second harmonic
Inlet guide vanes	bees accessed	59	rential s	au Liere e
nea get silence 000	Ok vie 4 in Exongor	44	Letreren	60d
First rotor	3		51	
I Bi Tripalle Sin e Segue	4			42.5
First stator	no bening to E ear	orrater In tel	50	
sel gotheld shi s	s with 6 a bar of	49	mss_sm_sgm	89
vestigation indica	ni aldu 7.15 hogu r	41.5	i ni.iga	
Second rotor	by the grmonics	perference area	JE LILL ST	56
	mi small 4 msq abo	yog oon os a	edd_beal	40.5
	evewoH 5 Patretan	the Inhade	52	on extend
	salt no 6 distants x	a lo remos	42	988B
Second stator	page 100 3 and vo	Lexining tell	. 70	46
Lo alouda enl' cu	mammasy 4 Tolymbo	g satt ment b	49.5	1 8-11- 1
Third rotor	10 0000 4 000 0000	lew arrivation	S.Edzawach (56.5
seasy housing anes	numos 5 of fishs	edde geed e	sonium et	45
y, greater interestor	catmatica neo	otgeralizerswi	49	127-11
Third stator	3		deranie n	62
the motor side	anoroli4 a mi La	not some mit me	dd 4454 64	46.5
	erdiv 05 noi0156e		50	0
	any of 6 he lote	Merra Mound of	46	ugli-est o
Fourth rotor	alled to 6 to behind	ay fills con	ONTO PAGE 1	51
of side alvily betition	por aspect 7 herory s	id hit theat to x	o called district	44
Fourth stator	4	nanceser off	de luiste	62.5
	5	dreilrindes .	seglian)	49.5
	6			41
Fifth rotor				
Fifth stator	7			49.5

The inlet guide vanes were the only blades to exhibit cracks evidently caused by vibrational stress. Aside from greater excitation force on the inlet guide vanes due to resonance at a higher compressor speed, the construction of inlet guide vanes rendered them more susceptible to fatigue. The guide vanes were formed sheet metal surfaces silver-soldered to their bases; the stator blades were machined from a solid block of metal and are consequently integral with the bases. In addition, the sharp corners and overhang of the guide vanes at the attachment to the blade base, as shown in figure 10, would make the inlet guide vanes much more susceptible to fatigue than were the first stage stators.

The compressor has been operated a total of 250 hours without a failure of the first stator; 50 to 75 hours of operation were at 50 percent of design speed. The length of time spent at conditions where resonance with the first stator was likely is not known accurately, but it probably exceeded 10 hours. This length of time is sufficient to cause failure if the vibratory stress has exceeded the endurance limit of the blade material, which was approximately 40,000 pounds per square inch.

The vibration data of reference 5 obtained on stator blades of approximately the same aspect ratio and solidity as the blading used in the inlet stages in the compressor used in this investigation indicate that the vibratory stress excited by the harmonics of the stall frequency was probably less than 20,000 pounds per square inch, or less than half the endurance limit of the blade material. However, it should be pointed out that the greatest source of excitation of the rotor blades from the progressive type stall exhibited by this compressor occurred near the rotor tips rather than near the point of attachment. The stator blades used in this investigation as well as those used in the investigation reported in reference 5 were attached to the compressor housing where the flow fluctuations were greatest. Consequently, greater vibratory stress at resonance with harmonics of the stall frequency may have occurred in rotors than in stators. In addition, the rotor blades are subject to centrifugal stress in addition to vibratory stress. Inasmuch as no fatigue cracks were found in any of the rotor blades after 250 hours of operation, it is concluded that the stresses due to any resonant vibrations excited in the rotor blades combined with the low centrifugal stress at the resonant conditions were of insufficient amplitude to fatigue the blades.

Surge

The term surge is used herein to define audible flow fluctuations that are axially symmetric as contrasted with the flow fluctuations of rotating stall which are caused by low flow stall regions revolving about the compressor axis.

Surge investigation. - The investigation of surge reported herein was confined to 50 percent of design speed. Attempts were made to obtain surge data with hot-wire anemometers at 60 and 70 percent of design speed, but in most cases the wire element of the probes was broken during a single surge pulse.

The variation in inlet stagnation pressure (axial station 1, fig. 1), discharge stagnation pressure (axial station 23), and hot-wire anemometer output at the tip radial station (radial station A) behind the first rotor (axial station 2) during several surge pulses is shown in figure 11.

The maximum decrease in compressor discharge pressure during a surge pulse divided by the compressor pressure rise at the surge point was 0.75. The maximum amplitude of the fluctuation in the inlet stagnation pressure divided by inlet pressure $\Delta P_{\rm S}/P_{\rm 0}$ was 0.1 and there were four damped pressure waves per surge pulse. Evidently these pressure waves in the inlet system were caused by the sudden reduction in weight flow rate ρV at the beginning of the surge pulse, as indicated by the hot-wire anemometer trace. Note that the weight flow rate was maximum when the compressor discharge pressure was a minimum and exceeded the value of weight flow rate prior to the surge pulse.

Motion pictures of the hot-wire anemometer output were taken during surge. Strips of these motion pictures showing the weight flow rate variation with time at three radial positions behind the first rotor (radial positions A, C, and E at axial station 2) are shown in figure 12. The left end of each film shows the fluctuations of rotating stall with frequency $f_{\rm S}$ of 340 cycles per second with λ = 7. The larger fluctuations that occur as the weight flow begins to drop indicate a change in type of stall.

The data indicate that the relatively low frequency surge was instigated by a stall region extending over the entire radial distance from blade tip to blade root with a stall frequency fg of about 30 cycles per second. Also, this root-to-tip stall results in a discontinuous drop in stage pressure ratio and consequently in the over-all compressor pressure ratio. That it is this discontinuous drop in compressor pressure rise that causes the compressor to surge is suggested in reference 7. With this compressor it appears that, at the lowest weight flow rate obtained during the surge pulse, the single stall region had spread out to cover the complete compressor annulus. As the weight flow rate increases during the surge pulse the compressor discharge pressure continues to decrease, as shown in figure 11. When the weight flow rate at all radial stations except radial station A had exceeded the value prior to the surge pulse, a sharp increase in weight flow rate was indicated just as the compressor discharge pressure reached a minimum. As the weight flow rate decreased again, the fluctuations of rotating stall with three stall zones and a frequency fg of 140 cycles per second appeared on the film. The weight flow rate continued to drop and the compressor discharge pressure to increase to the value prior to the surge pulse, and then the cycle repeated.

Strips of motion pictures of the oscilloscope taken during surge showing the hot-wire anemometer output from probes located behind the first rotor (axial station 2), behind the third stator (axial station 7), behind the seventh stator (axial station 15), and behind the tenth stator (axial station 22) are shown in figure 13. In all cases the probes were at the radial station A (see table I), and the upper trace of each film strip is the output of the anemometer behind the first rotor (axial

station 2). Each oscillogram shows the fluctuations of rotating stall with frequency $f_{\rm S}$ of 340 cycles per second and λ of 7 at the left end of the figure and the large rotating stall (root-to-tip stall) at the beginning of the surge pulse. The sharp rise in weight flow rate indicated near the center of each oscillogram is also in evidence at all axial stations except behind the first rotor.

The information obtained was insufficient to determine which stage initiated the single stall pattern due to root-to-tip stall. Although several oscillograms were studied, no definite conclusion can be drawn. As a stall region forms it evidently spreads axially and circumferentially while rotating about the compressor axis. Inasmuch as the anemometer probes at the various axial stations were each in a different meridional plane, the first probe to indicate the stall region depended upon the circumferential position at which the stall region started its formation.

Figure 14 shows the development of the large stall region at the beginning of the surge pulse in somewhat more detail than do figures 12 and 13. The upper trace is from an anemometer probe behind the fifth rotor and the lower trace, from a probe behind the first rotor ($\alpha = 185^{\circ}$). For these oscillograms the film speed was increased. In figure 14 the first large stall region to pass an anemometer probe appeared in an early stage of development behind the fifth rotor, but is shown slightly later in time (time required for approximately 1/2 revolution of stall region about compressor axis) well developed on the trace obtained from behind the first rotor (lower trace). By the time the stall region had made another 1/2 revolution about the compressor axis and encountered the probe in the fifth stage again, it had spread circumferentially to cover practically the complete annulus. Although the data did not indicate which stage initiated the root-to-tip stall, the data of reference 4 and the discussion of reference 7 suggest that root-to-tip stall is more likely to occur in the high hub-tip ratio stages used in the rear half of the compressor than in the inlet stages.

Discussion of Surge

The hot-wire anemometer data obtained during surge suggest that the flow fluctuations of surge are the result of cyclic stall and stall recovery, as discussed in reference 7. The surge cycle is illustrated in figure 15, showing the discontinuous drop in pressure ratio at stall and the discontinuous rise in pressure ratio at stall recovery. Inasmuch as a discontinuous drop in the compressor's ability to develop pressure due to root-to-tip stall results in a momentary unbalance of receiver pressure, compressor stall results in a flow transient as shown in figures 11 to 13. The sequence of events shown in figures 11 to 13 indicates the formation of the single stall zone due to root-to-tip stall, followed by a reduction in flow rate due to the momentarily

excessively high receiver pressure. The flow rate then overshoots the value prior to stall and stall recovery occurs. Stall recovery results in a sudden increase in flow rate due to the fact that the receiver pressure has fallen somewhat by the time stall recovery occurs. Following stall recovery the compressor discharge pressure increases and the flow rate decreases until conditions at the stall point are reestablished. Stall again occurs and the surge pulse is repeated.

The data of reference 4 and the discussion in reference 7 indicate that the amplitude of the flow variations during the transient following stall depends on the volume of the receiver into which the compressor is discharging. The multistage compressor data of reference 4 show that operation with a large receiver volume resulted in a sufficient weight flow rate overshoot during the transient following stall to effect stall recovery and consequently surge, whereas the flow transient following stall in operation with a small receiver was insufficient to cause stall recovery. This dependence on receiver volume is discussed in some detail in reference 7. The effect is further illustrated by the jet-engine data of references 12 and 13, which indicate compressor stall without surge. Presumably, the burner volumes used were sufficiently small to prevent stall recovery during the flow transient following stall.

SUMMARY OF RESULTS

The results of the hot-wire anemometer investigation of the flow fluctuations of stall in an NACA 10-stage research compressor at compressor speeds of 50, 60, and 70 percent of design speed and of surge at 50 percent of design speed may be summarized as follows:

- 1. At 50 percent of design speed, the flow fluctuations of rotating stall were found at the largest weight flow investigated. As the weight flow was reduced the number of stall regions in the pattern changed from a minimum of three to a maximum of seven near the surge point. At 60 percent of design speed only the stall patterns with three and four stall regions were obtained, and at 70 percent speed only the stall pattern with three stall regions was found.
- 2. For all stall patterns obtained the stall regions had a rotative speed of approximately 57 percent of the rotor speed, and stall regions pass through the compressor in the axial direction with little, if any, spiral motion.
- 3. The amplitude of the flow fluctuations of stall was greatest in the first four stages; but fluctuations were present in the tenth stage, and the amplitude of the fluctuations in the inlet stages varied somewhat with radius. The stage or stages initiating the rotating stall were not identified.

4. An analysis of the possibility of compressor blade vibration indicated that only the inlet guide vanes and first stator were in danger of resonant vibration with the fundamental frequency of the stall pattern. Other blade rows may have been in resonance with the first or second harmonic of the fundamental. Only the inlet guide vanes, however, suffered from a fatigue failure.

5. The hot-wire anemometer and pressure transducer data obtained during surge at 50 percent of design speed indicate that the surge pulse is initiated by a general breakdown of the flow in the compressor which results in a stall pattern with a single stall region which extends from compressor inlet to discharge. At the minimum flow during the surge pulse the stall region had spread to cover the complete annulus of the compressor. The weight flow then increased to a value greater than that at stall at which time the weight flow suddenly increased further due to stall recovery and then gradually decreased to the value for stall; the cycle was then repeated. The compressor discharge pressure drop during a surge pulse was 75 percent of the compressor pressure rise prior to surge.

Lewis Flight Propulsion Laboratory
National Advisory Committee for Aeronautics
Cleveland, Ohio

APPENDIX A

CALCULATION OF ROTATING STALL PATH FROM STAGE TO STAGE

In addition to calculating the number of stalls present in the compressor, it is of interest in an investigation of a multistage compressor to know the twist of the path of the rotating stall region along the axis of the compressor. As described in reference 4, the number of stalls in any particular stage may be calculated from a knowledge of the angular displacement between the hot-wire anemometers and the phase shift of the corresponding traces on the oscillogram. Similarly, it is possible to calculate the spiral of a rotating stall region as it extends through the compressor from a particular peripheral reference position.

If in figure 16 rotating stall region a is detected by wire 1, the rotating stall region at axial distance z downstream of wire 1 may have spiraled some angular displacement ϵ from the original position upstream. The detection of rotating stall region a by wire 2' displaced α degrees from wire 1 results in a phase shift X' of the hotwire anemometer traces on the oscillogram as shown in figure 19(a). If the hot-wire anemometers had been in the same stage, say at z = 0, and displaced α degrees, a time increment X between the appearance of the stall region on one probe and its appearance on the other probe would be found, as described in reference 4. This shift is shown by the dashed curve in figure 17(a).

The relation of the rate of this time increment to the stall period $1/f_{\rm S}$ is

$$Y = Xf_S$$
 or $Y'' = X''f_S$

and the ratio of the angular displacement between hot-wire anemometers and the angle between rotating stalls α/ν is a linear one, as shown in figure 19(b), and the line has a slope of 1. The difference between the value Y", representing the phase shift in the case of hot-wire anemometers z axial distance apart, and Y, representing what the phase shift would have been had the hot-wire anemometers been in the same plane, is a measure of the spiraling of the stall region. Since both Y" and Y against α/ν are linear and $\frac{\mathrm{d} Y}{\mathrm{d}(\alpha/\nu)} = \frac{\mathrm{d} Y''}{\mathrm{d}(\alpha/\nu)} = 1$, $Y - Y'' = \varepsilon/\nu$, as shown in figure 19(b). The example shown is for ε measured as positive in the direction of stall rotation. The determination of a rotating stall region spiral can be made as shown previously from a knowledge of the rotating stall phase shift between two hot-wire anemometers in a reference stage and in some stage axial distance z downstream.

APPENDIX B

DETERMINATION OF FUNDAMENTAL FREQUENCY OF COMPRESSOR

BLADES IN BENDING

The fundamental bending frequency of the blades in each blade row was determined by exciting a number of blades in a particular blade row to resonance with a magnetic exciter and determining the average frequency among those blades. A list of the average of the fundamental frequencies of the blades in each blade row is given in table II.

The fundamental bending frequency of the rotor blades is increased by the stiffening effect of the angular velocity of rotation. The ratio of the fundamental bending frequency with compressor rotation $(f_b)_n$ to that with no rotation $(f_b)_{\rm st}$ is given by reference 14 as

$$\left[\frac{(\mathbf{f}_b)_n}{(\mathbf{f}_b)_{st}}\right]^2 = 1 + \left[\frac{\beta N}{(\mathbf{f}_b)_{st}}\right]^2$$

The factor β depends on the taper and the ratio of hub radius to blade length. The rotor blades used in the compressor under investigation were not tapered and the hub-tip ratio of the blades at midchord was determined from information presented in reference 9. The appropriate values of β for each rotor blade were taken from the table on page 386 of reference 14.

REFERENCES

- 1. Finger, Harold B., and Dugan, James F., Jr.: Analysis of Stage Matching and Off-Design Performance of Multistage Axial-Flow Compressors. NACA RM E52D07, 1952.
- 2. Schulze, Wallace M., Erwin, John R., and Westphal, Willard R.: Investigation of an Impulse Axial-Flow Compressor Rotor over a Range of Blade Angles. NACA RM L50F27a, 1950.
- 3. Grant, Howard P.: Hot-Wire Measurements of Stall Propagation and Pulsating Flow in an Axial Flow Inducer-Centrifugal Impeller System. Pratt and Whitney Res. Rep. No. 133, June 1951.
- 4. Huppert, Merle C.: Preliminary Investigation of Flow Fluctuations During Surge and Blade Row Stall in Axial-Flow Compressors.

 NACA RM E52E28, 1952.

- 5. Huppert, Merle C., Johnson, Donald F., and Costilow, Eleanor L.:
 Preliminary Investigation of Compressor Blade Vibration Excited by
 Rotating Stall. NACA RM E52J15, 1952.
- 6. Medeiros, Arthur A., Benser, William A., and Hatch, James E.:
 Analysis of Off-Design Performance of a 16-Stage Axial-Flow Compressor with Various Blade Modifications. NACA RM E52L03, 1953.
- 7. Huppert, Merle C., and Benser, William A.: Some Stall and Surge Phenomena in Axial-Flow Compressors. Paper presented at Twenty-First Inst. Aero. Sci. meeting, New York (N. Y.), Jan. 26-29, 1953.
- 8. Johnsen, Irving A.: Investigation of a 10-Stage Subsonic Axial-Flow Research Compressor. I Aerodynamic Design. NACA RM E52B18, 1952.
- 9. Budinger, Ray E., and Thomson, Arthur R.: Investigation of a 10-Stage Subsonic Axial-Flow Research Compressor. II Preliminary Analysis of Over-All Performance. NACA RM E52CO4, 1952.
- 10. Laurence, James C., and Landes, L. Gene: Auxiliary Equipment and Techniques for Adapting the Constant-Temperature Hot-Wire Anemometer to Specific Problems in Air-Flow Measurements. NACA TN 2843, 1952.
- 11. Manley, R. G.: Waveform Analysis. John Wiley & Sons, Inc., 1945.
- 12. Goldstein, Arthur W., Alpert, Sumner, Beede, William, and Kovach, Karl: Analysis of Performance of Jet Engine from Characteristics of Components. II Interaction of Components as Determined from Engine Operation. NACA Rep. 928, 1949. (Supersedes NACA TN 1701.)
- 13. Conrad, E. William, Bloomer, Harry E., and Sobolewski, Adam E.:
 Altitude Operational Characteristics of a Prototype Model of the
 J47D (RX1-1 and RX1-3) Turbojet Engines with Integrated Electronic
 Control. NACA RM E51E08, 1952.
- 14. Timoshenko, Stephen: Vibration Problems in Engineering. Second ed., D. Van Nostrand Co., Inc., 1937.

TABLE I. - LOCATIONS OF DATA SURVEYS

Axial station	Preceding blade row	Radial position, ratio of radius to tip radius, r		
		A Tip	C Mean	E Hub
2	First rotor	0.97	0.82	0.64
3	First stator	.97	.83	.66
5	Second stator	.97	.85	.71
7	Third stator	.98	.87	.75
9	Fourth stator	.98	.89	.79
10	Fifth rotor	.98	.90	.81
15	Seventh stator	.98	.93	.89
22	Tenth stator	.98	.96	.94

TABLE II. - AVERAGE FUNDAMENTAL BENDING FREQUENCIES

Blade row	Natural frequency fb	Blade row	Natural frequency (f _b) _{st}
Inlet guide vanes	168	First rotor	250
First stator	284	Second rotor	322
Second stator	376	Third rotor	444
Third stator	532	Fourth rotor	618
Fourth stator	714	Fifth rotor	664
Fifth stator	1016	Sixth rotor	1216
Sixth stator	1452	Seventh rotor	1794
Seventh stator	2126	Eighth rotor	2576
Eighth stator	2946	Ninth rotor	3572
Ninth stator	4360	Tenth rotor	5690
Tenth stator	6030		
Exit guide vanes	6370		

NACA

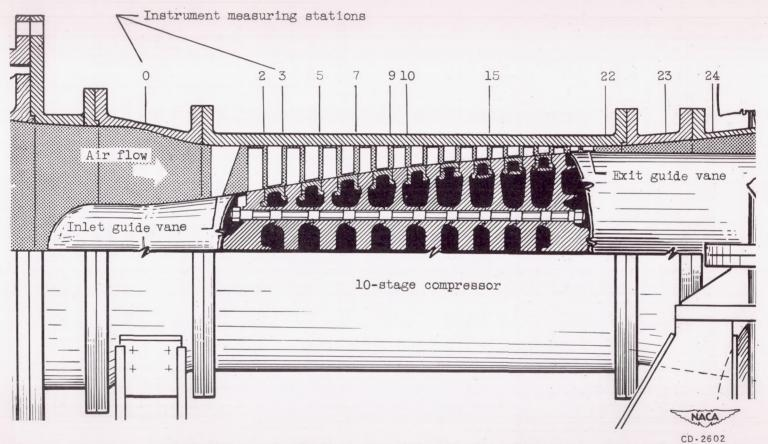


Figure 1. - Compressor cross section showing measuring stations.

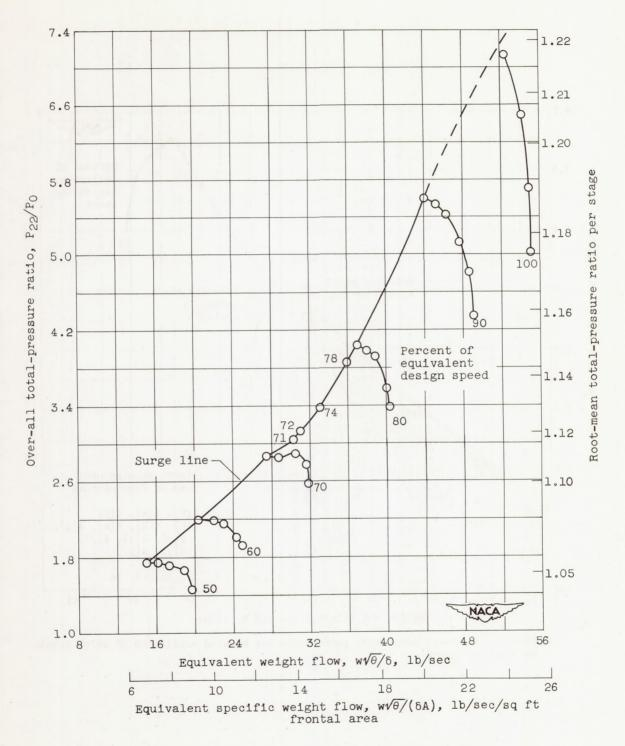


Figure 2. - Over-all compressor performance map.

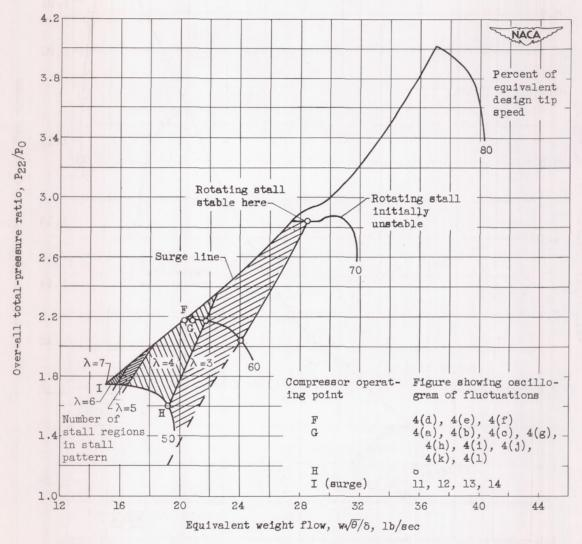
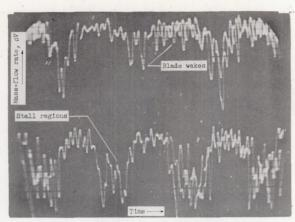
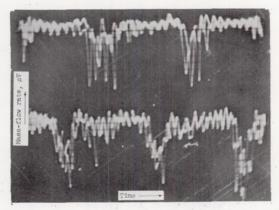


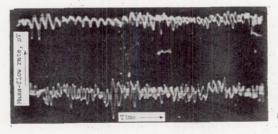
Figure 3. - Over-all compressor performance map showing conditions at which rotating stall occurred.



(a) Hot-wire anemometer at compressor casing (radial position A) and compressor operating at point G (fig. 3). Upper trace after first rotor (station 2, fig. 1), $\Delta\rho V/\overline{\rho V}=1.12$; lower trace after third stator (station 7, fig. 1), $\Delta\rho V/\overline{\rho V}=1.43$.



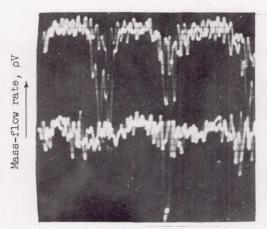
(b) Hot-wire anemometer at compressor mean radius (radial position C) and compressor operating at point G (fig. 3). Upper trace after first rotor (station 2, fig. 1), $\Delta\rho V/\rho \overline{V}=1.10$; lower trace after third stator (station 7, fig. 1), $\Delta\rho V/\rho \overline{V}=1.16$.





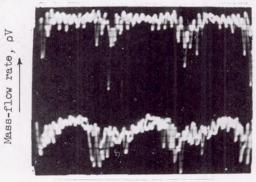
(c) Hot-wire anemometer at compressor hub (radial position E) and compressor operating at point G (fig. 3). Upper trace after first rotor (station 2, fig. 1), $\Delta\rho V/\rho \overline{V}=0.31$; lower trace after third stator (station 7, fig. 1), $\Delta\rho V/\rho \overline{V}=0.40$.

Figure 4. - Hot-wire anemometer oscillograms of rotating stall at three radii and various axial positions in compressor. Compressor rotative speed, 60 percent of design speed; stall pattern λ, 4; stall frequency f_s, 228 cycles per second.

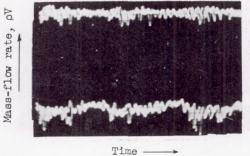


Time

(d) Hot-wire anemometer at compressor casing (radial position A) and compressor operating at point F (fig. 3). Upper trace after first rotor (station 2, fig. 1), $\Delta \rho V/\rho \overline{V} = 0.97$; lower trace after fifth rotor (station 10, fig. 1), $\Delta \rho V/\rho \overline{V} = 0.61$.



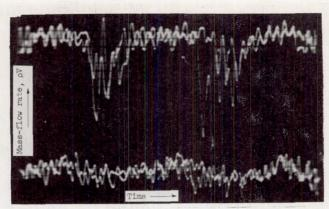
(e) Hot-wire anemometer at compressor mean radius (radial position C) and compressor operating at point F (fig. 3). Upper trace after first rotor (station 2, fig. 1), $\Delta \rho V/\rho \overline{V} = 0.75$; lower trace after fifth rotor (station 10, fig. 1), $\Delta \rho V/\rho \overline{V} = 0.60$.



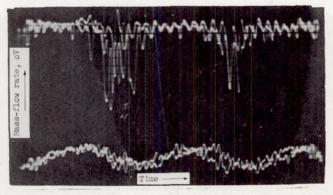
C-32510

(I) HOT-Wire anemometer at compressor hub (radial position E) and compressor operating at point F (fig. 3). Upper trace after first rotor (station 2, fig. 1), $\Delta \rho V/\rho V = 0.30$; lower trace after fifth rotor (station 10, fig. 1), $\Delta \rho V/\rho \overline{V} = 0.42$.

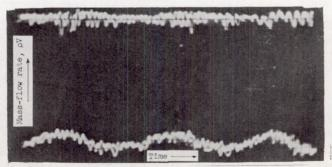
Figure 4. - Continued. Hot-wire anemometer oscillograms of rotating stall at three radii and various axial positions in compressor. Compressor rotative speed, 60 percent of design speed; stall pattern λ , 4; stall frequency f_s , 228 cycles per second.



(g) Hot-wire anemometer at compressor casing (radial position A) and compressor operating at point G (fig. 3). Upper trace after first rotor (station 2, fig. 1), $\Delta\rho V/\rho V=1.13$; lower trace after seventh stator (station 15, fig. 1), $\Delta\rho V/\rho V=0.56$.



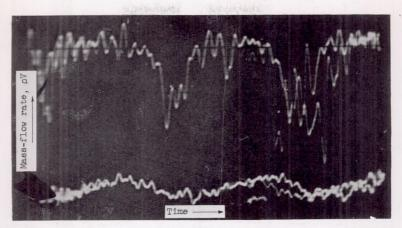
(h) Hot-wire anemometer at compressor mean radius (radial position C) and compressor operating at point G (fig. 3). Upper trace after first rotor (station 2, fig. 1), $\Delta \rho V/\rho \overline{V} = 0.85$; lower trace after seventh stator (station 15, fig. 1), $\Delta \rho V/\rho \overline{V} = 0.53$.



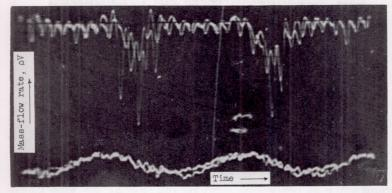
NACA C-32511

(i) Hot-wire anemometer at compressor hub (radial position E) and compressor operating at point G (fig. 3). Upper trace after first rotor (station 2, fig. 1), $\Delta\rho V/\bar{\rho V}=0.28$; lower trace after seventh stator (station 15, fig. 1), $\Delta\rho V/\bar{\rho V}=0.30$.

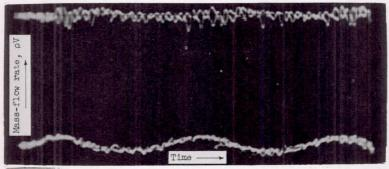
Figure 4. - Continued. Hot-wire anemometer oscillograms of rotating stall at three radii and various axial positions in compressor. Compressor rotative speed, 60 percent of design speed; stall pattern λ , 4; stall frequency f_s, 228 cycles per second.



(j) Hot-wire anemometer at compressor casing (radial position A) and compressor operating at point G (fig. 3). Upper trace after first rotor (station 2, fig. 1), $\Delta\rho V/\rho \overline{V}=1.14$; lower trace after tenth stator (station 22, fig. 1), $\Delta\rho V/\rho \overline{V}=0.51$.



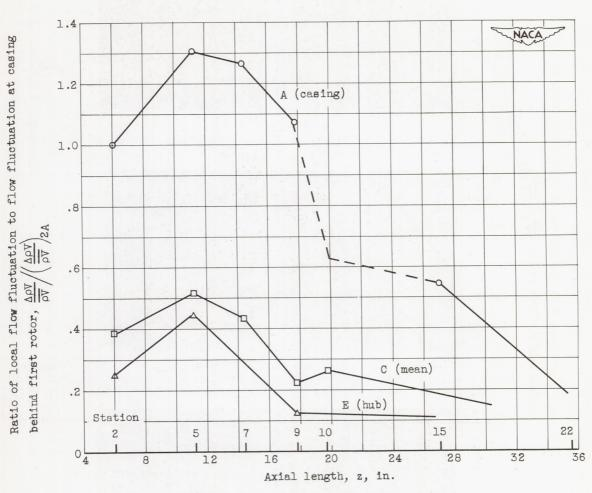
(k) Hot-wire anemometer at compressor mean radius (radial position C) and compressor operating at point G (fig. 3). Upper trace after first rotor (station 2, fig. 1), $\Delta\rho V/\rho \overline{V} = 0.74$; lower trace after tenth stator (station 22, fig. 1), $\Delta\rho V/\rho \overline{V} = 0.43$.



NACA C-32512

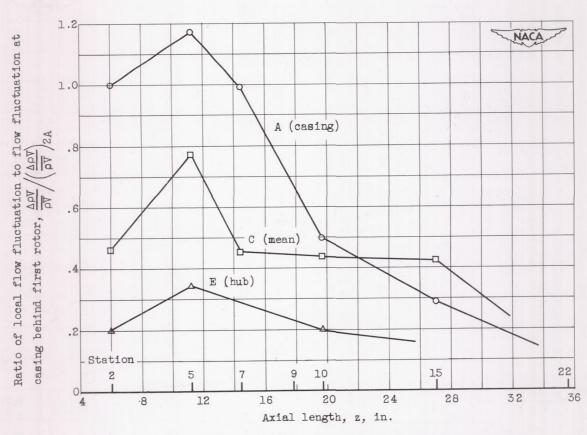
(1) Hot-wire anemometer at compressor hub (radial position E) and compressor operating at point G (fig. 3). Upper trace after first rotor (station 2, fig. 1), $\Delta\rho V/\overline{\rho V}=0.32$; lower trace after tenth stator (station 22, fig. 1), $\Delta\rho V/\overline{\rho V}=0.39$.

Figure 4. - Concluded. Hot-wire anemometer oscillograms of rotating stall at three radii and various axial positions in compressor. Compressor rotative speed, 60 percent of design speed; stall pattern λ , 4; stall frequency f_s , 228 cycles per second.



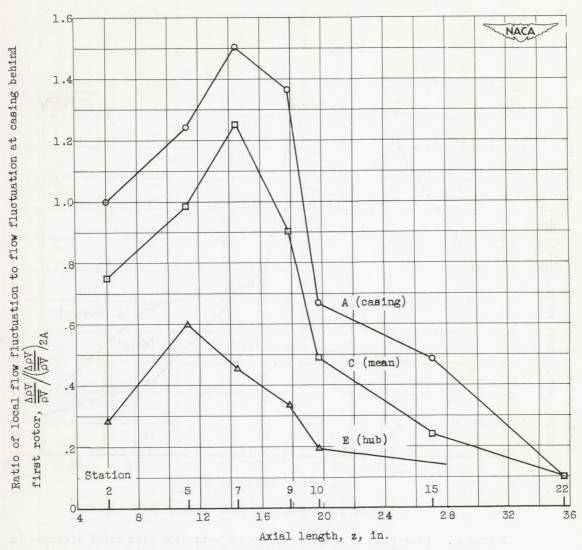
(a) Stall frequency f_S , 142; stall pattern λ , 3.

Figure 5. - Variation in flow fluctuation with axial distance in compressor at three radii for compressor rotative speed 50 percent of design speed.



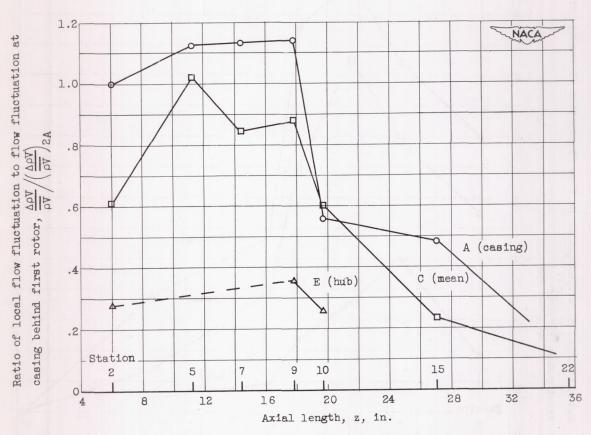
(b) Stall frequency f_S , 190; stall pattern λ , 4.

Figure 5. - Continued. Variation in flow fluctuation with axial distance in compressor at three radii for compressor rotative speed 50 percent of design speed.



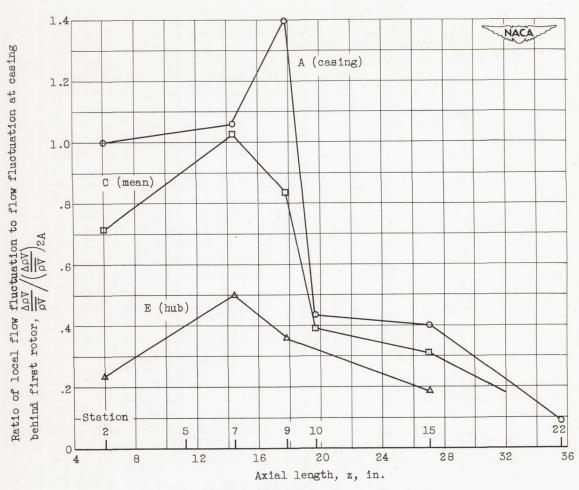
(c) Stall frequency $\,f_{\mbox{\scriptsize S}},\,\,240;$ stall pattern $\,\,\lambda,\,\,5\,.$

Figure 5. - Continued. Variation in flow fluctuation with axial distance in compressor at three radii for compressor rotative speed 50 percent of design speed.



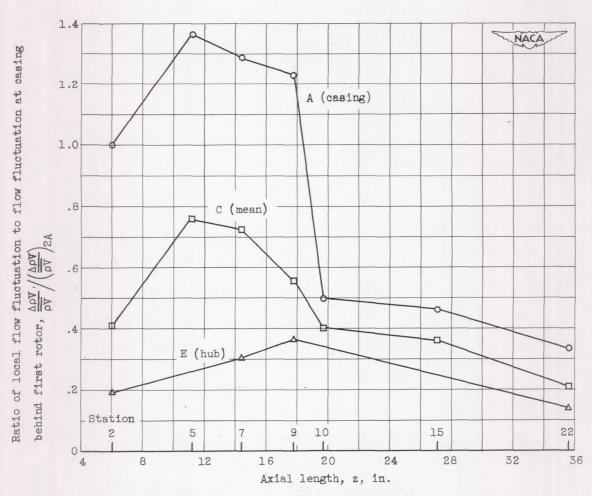
(d) Stall frequency f_S , 290; stall pattern λ , 6.

Figure 5. - Continued. Variation in flow fluctuation with axial distance in compressor at three radii for compressor rotative speed 50 percent of design speed.



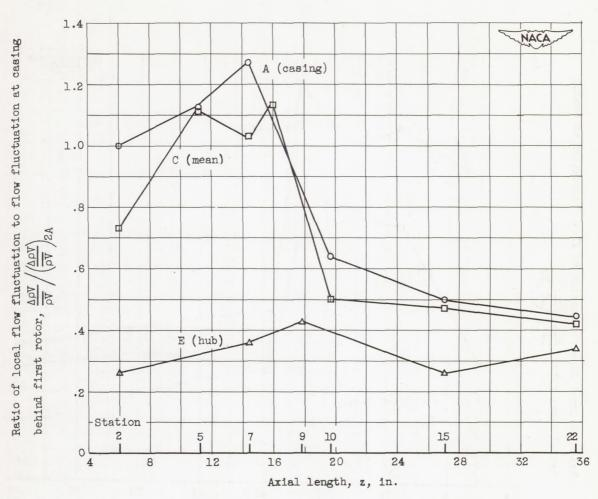
(e) Stall frequency $f_{\rm S}$, 340; stall pattern λ , 7.

Figure 5. - Concluded. Variation in flow fluctuation with axial distance in compressor at three radii for compressor rotative speed 50 percent of design speed.



(a) Stall frequency f_S , 168; stall pattern λ , 3.

Figure 6. - Variation in flow fluctuation with axial distance in compressor at three radii for compressor rotative speed 60 percent of design speed.



(b) Stall frequency f_S , 228; stall pattern λ , 4.

Figure 6. - Concluded. Variation in flow fluctuation with axial distance in compressor at three radii for compressor rotative speed 60 percent of design speed.

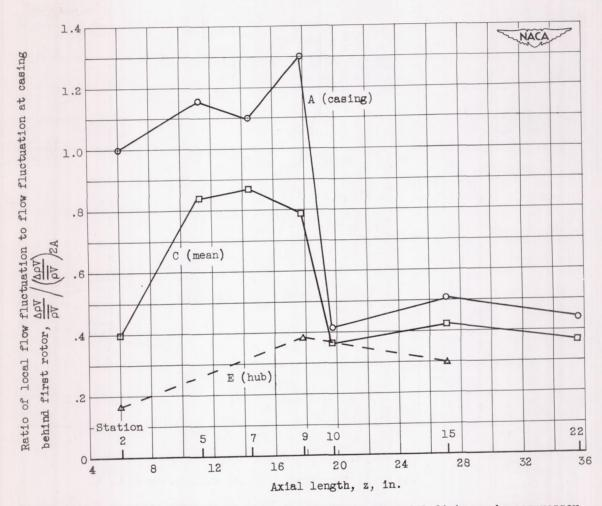
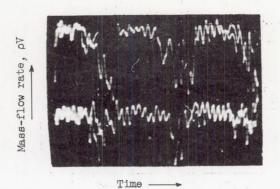
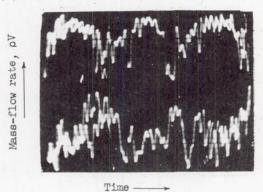


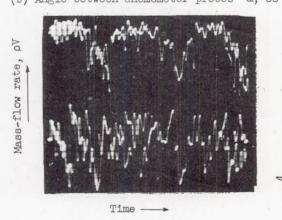
Figure 7. - Variation in flow fluctuation with axial distance in compressor at three radii for compressor rotative speed 70 percent of design speed.



(a) Angle between anemometer probes α , 86°.



(b) Angle between anemometer probes α , 88°.



(c) Angle between anemometer probes α , 92° .

C-32513

Figure 8. - | Hot-wire anemometer oscillogram showing circumferential survey through angular positions after first stator. Radius ratio r, 0.9; stall pattern λ , 4; stall frequency f_8 , 190 cycles per second; compressor rotative speed 50 percent of design speed; and compressor operating point H (fig. 3).

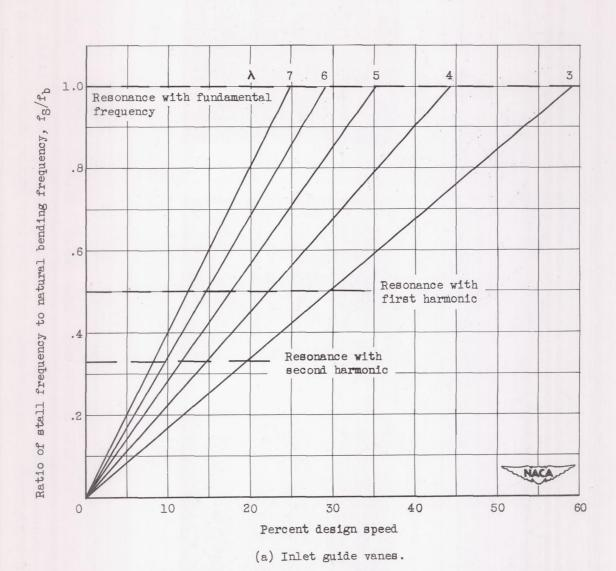


Figure 9. - Variation of ratio of stall frequency to natural bending frequency with percent design speed.

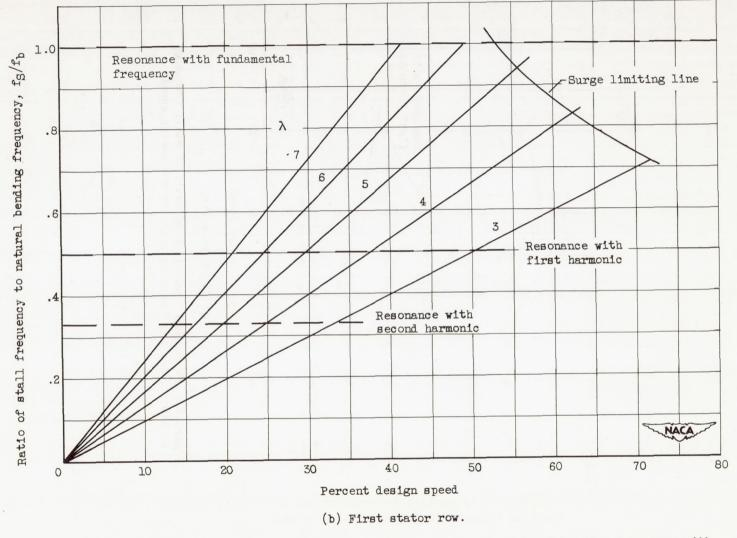
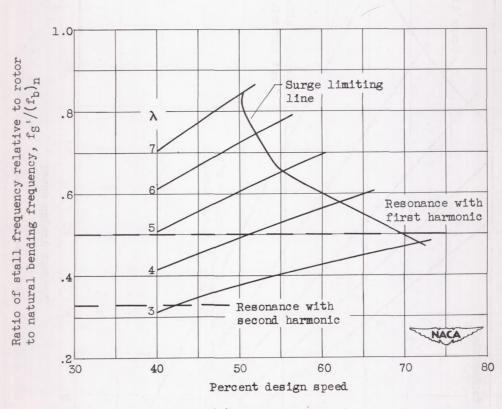


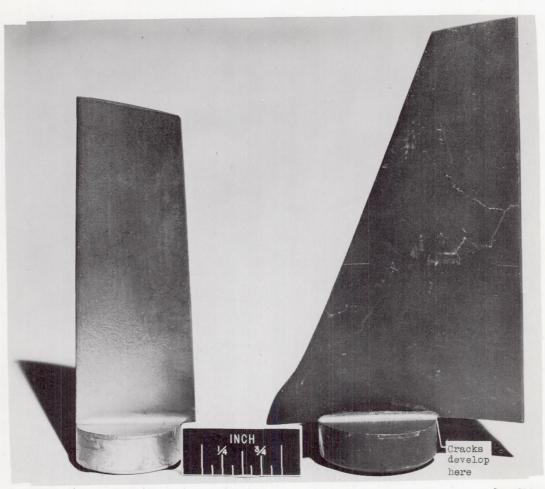
Figure 9. - Continued. Variation of ratio of stall frequency to natural bending frequency with percent design speed.



(c) First rotor row.

Figure 9. - Concluded. Variation of ratio of stall frequency to natural bending frequency with percent design speed.

NACA RM E53Cl9

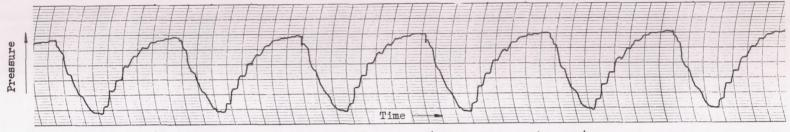


Stator blade

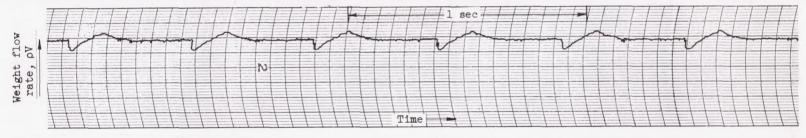
Inlet guide vane



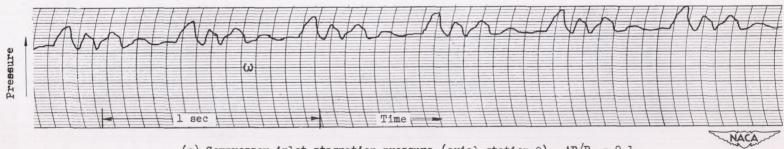
Figure 10. - First stator blade and inlet guide vane.



(a) Compressor discharge stagnation pressure (axial station 24). $\Delta P_{\rm S}/\Delta P_{\rm c}$ = 0.75.

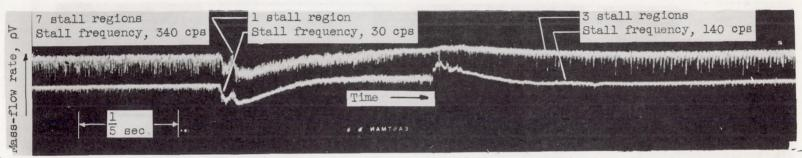


(b) Hot-wire anemometer behind first rotor at compressor casing (radial position A).

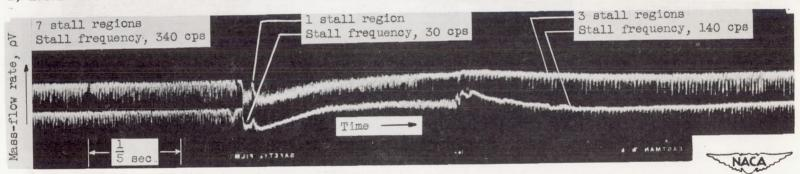


(c) Compressor inlet stagnation pressure (axial station 0). $\Delta P/P_0$ = 0.1.

Figure 11. - Variation in compressor inlet and discharge stagnation pressures and weight flow rate during surge at 50 percent of design speed. Compressor operating point I (fig. 3); surge frequency, 0.57 cycle per second.

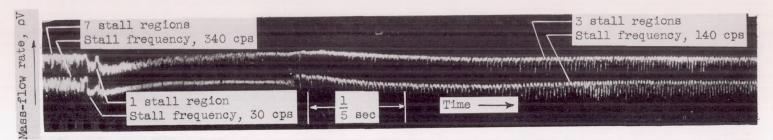


a) Lower trace at hub radial station (radial position E); upper trace at tip radial station (radial position A),

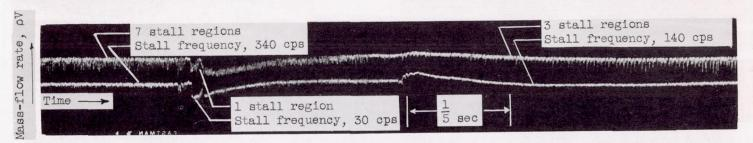


(b) Lower trace at mean (radial station C); upper trace at tip (radial position A). C-32514

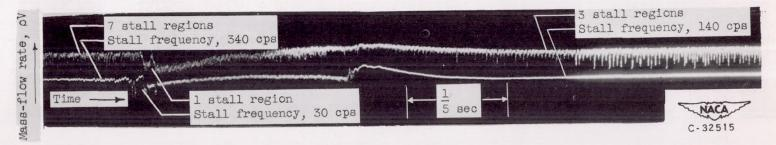
Figure 12. - Oscillograms of flow fluctuations of surge at three radial positions behind first rotor. Compressor rotative speed 50 percent of design speed; angle between probes α , 20.3°; compressor operating point I (fig. 3); surge frequency, 0.57 cycle per second.



(a) Upper trace behind first rotor (station 2A); lower trace behind third stator (station 7A). Angle between probes α, 64.6°.

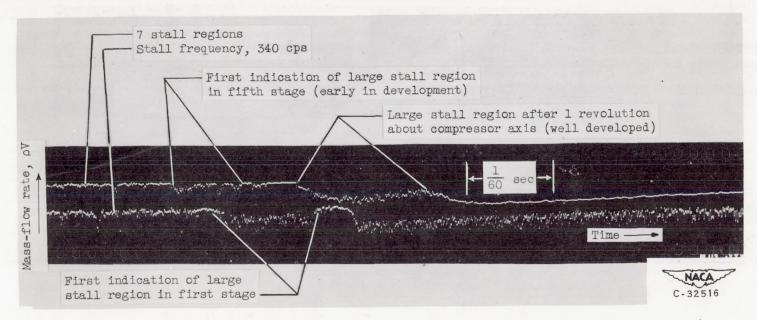


(b) Upper trace behind first rotor (station 2A); lower trace behind seventh stator (station 15A). Angle between probes α, 104.1°.



(c) Upper trace behind first rotor (station 2A); lower trace behind tenth stator (station 22A). Angle between probes α, 104.9°

Figure 13. - Oscillogram of surge at various axial stations. Anemometer probes at casing (radial position A) 50 percent of design speed. Compressor operating point I (fig. 3): surge frequency, 0.57 cycle per second.



Upper trace behind fifth rotor (axial station 10); lower trace behind first rotor (axial station 2).

Figure 14. - Oscillogram showing large rotating stall region at beginning of surge pulse. Anemometers behind first and fifth rotors; speed, 50 percent of design; surge frequency, 0.57 cycle per second; angle between probes α , 185°. Probes at casing (radial position A); compressor operating point I (fig. 3.).

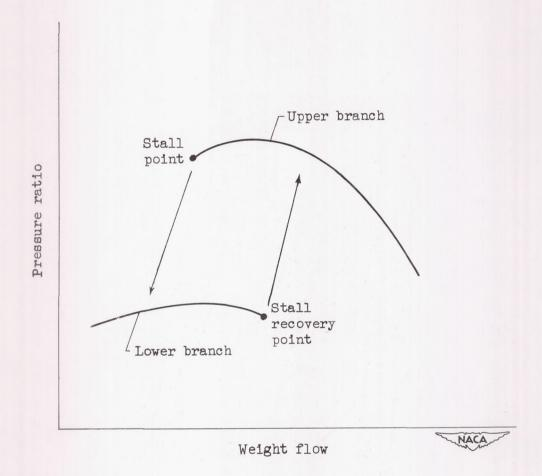


Figure 15. - Typical characteristic speed curve.

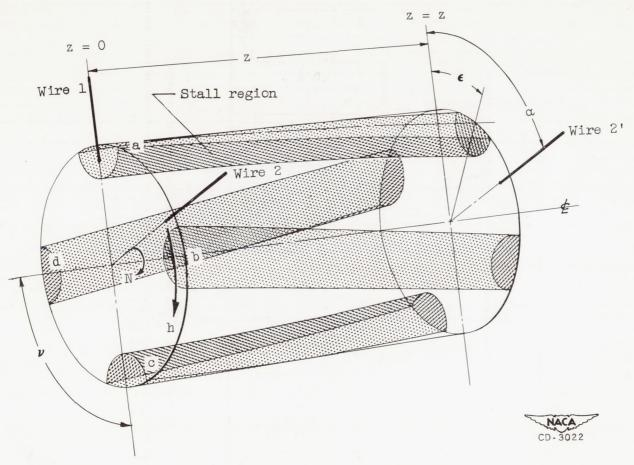
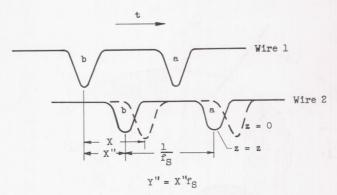
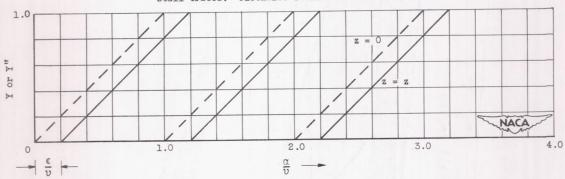


Figure 16. - Sketch indicating possible spiraling path of rotating stall regions.



(a) Oscillogram showing phase shift $\, X \,$ and $\, X \,$ of rotating stall traces. Clockwise stall rotation.



(b) Variation of Y and Y" with α/ν . Clockwise stall rotation.

Figure 17. - Relations necessary for determining spiraling path of rotating stall region.